Infrared study of the electronic structure of the metallic pyrochlore iridate Bi_{2}Ir_{2}O_{7}

Y. S. Lee, S. J. Moon, Scott C. Riggs, M. C. Shapiro, I. R. Fisher, Bradford W. Fulfer, Julia Y. Chan, A. F. Kemper, and D. N. Basov

Phys. Rev. B **87**, 195143 — Published 30 May 2013

DOI: 10.1103/PhysRevB.87.195143

Infrared study of the electronic structure of metallic pyrochlore iridate $Bi_2Ir_2O_7$

Y. S. Lee[1,2], S. J. Moon[1,3], Scott C. Riggs[4,5], M. C. Shapiro[4,5], I. R. Fisher[4,5], Bradford W. Fulfer[6], Julia Y. Chan[6], A.F. Kemper[7], and D. N. Basov[1]

[1]*Department of Physics, University of California at San Diego, La Jolla, CA 92093*

[2]*Department of Physics, Soongsil University, Seoul 156-743, Republic of Korea*

[3]*Department of Physics, Hanyang University, Seoul 133-791, Republic of Korea*

[4]*Department of Applied Physics and Geballe Laboratory for Advanced Materials, Stanford University, Stanford, California 94305*

[5]*Stanford Institute for Materials and Energy Science, SLAC National Accelerator Laboratory, Menlo Park, California 94025*

[6]*Department of Chemistry. Louisiana State University. Baton Rouge, LA 70803*

[7]*Scientific Computing Division Lawrence Berkeley National Laboratory, Berkeley, California 94720*

We investigated the electronic properties of a single crystal of metallic pyrochlore iridate $Bi_2Ir_2O_7$ by means of infrared spectroscopy. Our optical conductivity data show the splitting of t_{2g} bands into J_{eff} ones due to strong spin-orbit coupling. We observed a sizable mid-infrared absorption near 0.2 eV which can be attributed to the optical transition within the $J_{eff,1/2}$ bands. More interestingly, we found an abrupt suppression of optical conductivity in the very far-infrared region. Our results suggest that the electronic structure of $Bi_2Ir_2O_7$ is governed by the

strong spin-orbit coupling and correlation effects, which are prerequisite for theoretically proposed non-trivial topological phases in pyrochlore iridates.

PACS number: 78.20.-e, 71.30.+h, 71.20.-b

I. INTRODUCTION

Transition metal oxides (TMOs) have been the topic of intensive research due to wide range of enigmatic electronic properties [1]. The electron-electron correlations effects are believed to be the driving factor for intriguing phenomena observed in 3*d* TMOs; these include but are not limited to Mott transition, high-T_c superconductivity, and colossal magnetoresistance [2, 3]. In the case of 4*d* and 5*d* TMOs the on-site Coulomb repulsion energy U, becomes smaller than that in the 3*d* counterparts because 4*d* and 5*d* orbitals are spatially more extended. A distinguishing feature of 5*d* TMOs is that the energy scale of the spin-orbit coupling is comparable to U. In view of complex interplay between the electronic correlations and the spin-orbit coupling, the 5*d* TMO Ir-oxides have been intensively studied. Indeed, a plethora of perplexing phenomena have been discovered in 5*d* iridates such as a weakly correlated Mott state with magnetic instability [4], metal-insulator transition [5-7], charge density instability [8].

Recently, the pyrochlore iridates $R_2Ir_2O_7$ (R: rare-earth ions) have attracted much attention due to a metallic spin liquid behavior originating from generic geometrical frustration and possible topologically non-trivial states [9-16]. It was also pointed that the pyrochlore iridates could provide a unique opportunity to study electronic properties governed by electronic correlations, spin-orbit coupling, and band topology [13]. The strength of electronic correlations in $R_2Ir_2O_7$ system can be controlled by the size of R^{3+} ions which affects the effective bandwidth of the 5*d* Ir band by changing the Ir-O-Ir bond angle [17]. Indeed, the $R_2Ir_2O_7$ compounds show the insulator-to-metal transition with the increasing size of R from Y (or Gd – Lu) to Pr [14, 18-21]. With advantage of the tunability of their ground states, $R_2Ir_2O_7$ is emerging as a test bed for new theoretical ideas pertaining to non-trivial topological states such as correlated topological insulator and topological Weyl semimetal [13-16].

In this paper, we investigated the electronic structure of metallic pyrochlore $Bi_2Ir_2O_7$. We studied single crystal samples by means of infrared spectroscopy. So far, there have been few spectroscopic studies of electronic structure of pyroclore iridates [21,22] and no such data were reported for $Bi_2Ir_2O_7$. Very recently, high-quality single crystalline $Bi_2Ir_2O_7$ samples have become available for spectroscopic experiments. Our infrared (IR) data indicate the importance of electronic correlations and spin-orbit coupling for determining the electronic properties of $Bi_2Ir_2O_7$. Interband transitions above 1 eV in our optical data can be assigned in the scheme of electronic structure by taking account of strong spin-orbit coupling. The optical conductivity spectra of this compound show distinct mid-IR absorption near 0.2 eV, and, more interestingly, the abrupt suppression in the very-far-IR region. We discuss the relevance of our findings to the hypothesis of non-trivial topological states [13-16].

II. EXPERIMENT

Single crystals of $Bi_2Ir_2O_7$ were grown by a self-flux method, by slowly cooling a melt with a slight excess of Bi_2O_3. For the sample measured in this study, Bi_2O_3 (99.8 % pure) and IrO_2 (99.99% pure) were combined in a 50 ml Pt crucible in a molar ratio of 40:60 [23]. The reagents were placed in 50 ml Pt crucible and placed into furnace. The material was heated from room temperature to 850 °C for 10 hours, then to 1100 °C for 125 hours. The furnace was then allowed to cool back to 850 °C over 125 hours and then the crucible was decanted, and the furnace was allowed to cool down to room temperature. Crystals with dimensions up to approximately 400 μm were readily extracted from the crucible. The crystals have truncated octahedron morphology, with the [100] direction perpendicular to the square faces. There is no evidence of the material being sensitive to air. The synchrotron x-ray refinement revealed that our samples are of a single phase, and the crystalline structure is a cubic with the space group $Fd\bar{3}m$ [23]. Information on the structural properties is provided in the Appendix. The

lattice parameter is 10.3160(11) Å and 10.312(7) Å at 294 K and 150 K, respectively, which indicates that the lattice parameter changes negligibly with temperature variation. The details of sample preparation and characterization will be published elsewhere [24].

Electrical resistivity measurements were performed from 300 K to 1.4 K using a Quantum Design PPMS in the standard four probe geometry. To obtain reliable DC resistivity data, the measurements were performed for three samples with different sizes, including the same particular crystal used for infrared spectroscopy. We found the DC resistivity data of all the samples to be quite consistent. As shown in the inset of Fig. 2(a), the DC resistivity curve shows a positive slope with the increasing *T*, which is indicative of the metallic state of our sample. The metallic state of $Bi_2Ir_2O_7$ is expected because the ionic size of Bi^{3+} (1.17 Å) is larger than that of Pr^{3+} (1.126 Å) in a metallic compound $Pr_2Ir_2O_7$ [25]. In addition, the 6*p* orbital of Bi^{3+} lies near the Fermi level and hybridizes strongly with the Ir 5*d* bands, which makes the 5*d* bandwidth wider [26]. The residual resistivity ratio (RRR) is found to be 1.4. A similar RRR value, ~ 1.1 is found in another study on the $Bi_2Ir_2O_7$ thin films [27]. This small value is in accord with the weak temperature dependence of our reflectivity spectra which will be discussed later. The small RRR is also observed in $Bi_2Ru_2O_7$, a metallic 4*d* pyrochlore compound (RRR~1.2) [28].

Reflectivity spectra $R(\omega)$ at nearly normal incidence were measured at temperatures from 10 to 293 K. The surface area of the sample used for reflectivity measurement is about 0.4 x 0.4 mm^2. Due to the very small sample size, the measurement frequency range is limited to above 150 cm^{-1} (~ 0.02 eV). An in-situ gold coating technique was employed for reference spectra [29]. The complex optical conductivity spectra $\sigma(\omega)=\sigma_1(\omega)+\sigma_2(\omega)$ were obtained from the measured $R(\omega)$ using the Kramers-Kronig (KK) transformation.

III. RESULTS AND DISCUSSION

Figure 1 shows reflectance data for $Bi_2Ir_2O_7$. In Fig. 1(a), $R(\omega)$ spectra exhibit a high level in the far-infrared (IR) region and approach the unity at the lowest frequencies, which is indicative of the metallic state. The hump structure in $R(\omega)$ is observed in the mid-IR region near 0.4 eV, followed by gradual decrease of the reflectivity level with the increasing frequency up to 2 eV. Additionally, the high-energy peak structure is resolved near 3 eV. While we do not see any discernible temperature dependence in $R(\omega)$ above 1.0 eV, the far-IR reflectivity level becomes higher with decreasing temperature, as shown in the inset of Fig. 1(a). The overall temperature dependence in $R(\omega)$ is quite weak, which is consistent with the small RRR observed in our transport measurement.

Direct information of the electronic structure can be obtained in optical conductivity data that are derived from K-K transformation of $R(\omega)$. For the purpose of KK analysis, appropriate extrapolations of $R(\omega)$ are needed. Due to the limitation on the very far-IR measurement, we face ambiguities in extrapolating $R(\omega)$ to the zero frequency. The most common method of the reflectivity extrapolation for metallic compound is Hagen-Rubens (H-R) relation: $R(\omega) \sim 1 - \sqrt{\omega \rho_{DC} / \pi}$, where ρ_{DC} is the DC resistivity. We plotted the H-R lines calculated using the DC resistivity values obtained from the transport measurement (dot-dashed lines in Fig. 1(b)). A clear difference is found between the measured reflectivity values and the H-R lines near 0.02 eV. This discrepancy highlights highly unconventional low-frequency electrodynamics of $Bi_2Ir_2O_7$.

We examined a couple of different low-frequency extrapolation schemes for the KK transformation in order to discern possible role of extrapolations in the optical conductivity data. First we attempted to impose the H-R extrapolation. We note that the H-R relation is expected be valid only at very low frequencies below the scattering rate of mobile charge carriers [30]. We therefore assumed that the measured $R(\omega)$ meets the H-R lines near 0.001 eV: outside attainable experimental region (dashed lines in Fig. 1(b)). We extended the reflectivity curves below 0.02 eV, continuing the slope of the reflectivity spectra. At the lowest frequencies (below 0.001 eV) we employed the H-R form with the

measured ρ_{DC}. We denote this extrapolation procedure as EP1. An alternative procedure (denoted at EP2) involved the extension of the measured $R(\omega)$ with the H-R form (dotted lines in Fig.1(b)). However this latter procedure required an assumption of ρ_{DC} values that exceed experimental results by the factor between 4 and 5.

In Figs. 2 and 3 we display the optical conductivity data of $Bi_2Ir_2O_7$ obtained using both extrapolation methods, EP1 and EP2. We first note that ambiguities caused by extrapolations have only mild impact on the form of the conductivity spectra in the frequency region where actual data exist (Fig. 3(a)). None of the gross features seen in Fig. 2(a) are sensitive to extrapolations. The conductivity spectra reveal two interband transitions near 1.2 eV and above 3 eV; we labeled these features as 'Peak β' and 'Peak γ', respectively. We observe substantial spectral weight below 0.5 eV with a noticeable resonance near 0.2 eV, labeled as Peak α. The overall form of $\sigma_1(\omega)$ in $Bi_2Ir_2O_7$ is typical for TMOs: clear interband transitions and low-energy spectral weight [2, 3].

Figure 3 details the far-IR conductivity: the region where KK-generated spectra of $\sigma_1(\omega)$ depend on the choice of the low frequency extrapolation. We calculated the optical conductivity data with different extrapolations (EP1 and EP2), and displayed the calculated data in the measurement and extrapolation regions separately with the solid and dotted lines in Fig. 3(a), respectively. Apart from the difference in the absolute value of the conductivity (about 10 % at 0.02 eV), the overall features of $\sigma_1(\omega)$ are similar for either extrapolation. With decreasing temperature the conductivity in the far-IR region increases in accord with the metallic state of our sample. However, the magnitude of optical conductivity at the lowest measured frequencies are much higher than the DC conductivity (solid circles on the *y* axis) estimated from the transport measurement shown in the inset of Fig. 3(a): at 10 K, the $\sigma_1(\omega$=0.05 eV) =~ 5,000 $\Omega^{-1}cm^{-1}$ and σ_{DC} = ~1,000 $\Omega^{-1}cm^{-1}$. Obviously, one expects that the

frequency dependent optical conductivity extrapolates to the DC conductivity as the frequency goes to zero. In order to reconcile our DC and AC results, we are forced to conclude that there is a drastic suppression of the conductivity in the very far-IR and THz regions. Interestingly, this unusual behavior is well reproduced by the optical conductivity data obtained with the EP1 extrapolation. We note that the unusual electrodynamics without a coherent feature is one of characteristics of strongly correlated materials [3].

One possible origin of the very low frequency suppression in $\sigma_1(\omega)$ of $Bi_2Ir_2O_7$ is localization effects driven by disorder associated, for example, with oxygen or cation deficiencies. The diffusive transport due to the localization leads to the positive slope in $\sigma_1(\omega)$ from the zero frequency: a common occurrence in disordered transition metal oxides. [31-34]. In addition we note that the Bi ions in $Bi_2Ir_2O_7$ have the 6*s* lone electron pair. The lone pair may induce the displacement of Bi ions in random directions. This could lead to randomness of the hybridization between Bi 6*p* and Ir 5*d* orbitals [35,36].

As another possibility, we note that the similar unusual low-frequency behavior of the conductivity was recently observed for the polycrystalline $Nd_2(Ir,Rh)_2O_7$ [21]. The $\sigma_1(\omega)$ in the insulating phase of $Nd_2Ir_2O_7$ shows the drastic suppression below 0.1 eV. With increasing Rh ion concentration as the system becomes more metallic, this anomaly of the conductivity shifts down to about 0.04 eV. It was suggested that this behavior should be attributed to the topological Weyl semimetal phase [15], which has been theoretically proposed as a possible ground state of pyrochlore iridates [13-16]. The Weyl semimetal phase has linearly dispersing excitations at the Fermi level inside a three-dimensional system, described by "Weyl equation", i.e., the two component analog of the Dirac equation. Wan *et al*. first suggested that this Weyl semimetal phase could be realized in pyrochlore iridates [16]. In the semimetal phase where the charge gap is closed but the coherent peak is absent, the optical conductivity is predicted to increase as the frequency increases from $\omega = 0$. Therefore, the spectral

form of our far-IR conductivity data may suggest that the Weyl semimetal phase could be relevant for the ground state of $Bi_2Ir_2O_7$. We note that Qi *et al*. reported on non-Fermi liquid behavior of both electronic and thermodynamics properties of single crystalline $Bi_2Ir_2O_7$ [23], which might be also relevant to the non-trivial topological phase.

Even though the Weyl scenario of the optical absorption is appealing, it is nevertheless inconsistent with the suppression of the optical conductivity at $\omega > 0.1$ eV. As shown in Fig. 3, the low frequency peak with a sizable spectral weight may originate from electronic transitions unrelated to the Weyl semimetal state. Similar issue is relevant to the interpretation of data in Ref. [22]. Thus the Weyl scenario leaves unaccounted the low-frequency spectral weight observed in our experiments and also results reported in Ref. [22]. To clarify the lowest frequency electronic response of $Bi_2Ir_2O_7$, further experiments such as THz and photoemission spectroscopy studies on high-quality single crystalline samples with high-energy resolution are required.

We now turn to the discussion of the electronic structure of $Bi_2Ir_2O_7$. Since the valency of the Ir ions is 4+, there are five electrons for the Ir 5*d* orbitals. Due to the crystal-field splitting in the IrO_6 octahedron, the Ir 5*d* bands are divided into two bands, t_{2g} and e_g bands. The strong spin-orbit coupling further splits the t_{2g} bands into fourfold-degenerate $J_{\text{eff},3/2}$ and doubly-degenerate $J_{\text{eff},1/2}$ [4,14,22,23]. The former is located at a lower energy than the latter. Thus the $J_{\text{eff},3/2}$ band is fully occupied with four electrons and the $J_{\text{eff},1/2}$ band is half-filled. According to this scheme shown in Fig. 2(b), one expects two interband transitions, from the $J_{\text{eff},3/2}$ band to the $J_{\text{eff},1/2}$ and to e_g bands, respectively. We assign Peak β *to* $J_{\text{eff},3/2} \rightarrow J_{\text{eff},1/2}$ transition and Peak γ in our data to $J_{\text{eff},3/2} \rightarrow e_g$ transition. We emphasize that without strong spin-orbit coupling the two interband features would merge into a single transition from the t_{2g} to e_g bands. We therefore conclude the spin-orbit coupling plays a crucial role in determining the electronic structure of $Bi_2Ir_2O_7$.

In contrast to Peaks β and γ, the existence of Peak α is rather enigmatic. We found that Peak α is well fitted with a Lorentz oscillator located at 0.23 eV for the 10 K $\sigma_1(\omega)$. We also attempted to fit our IR data by using two Drude modes with different scattering rates, and found that this fitting does not fully account for the mid-IR absorption in our conductivity spectra. It is rather surprising that the well-defined resonance exists at such a low energy in the mid-IR. In many correlated materials the spectral weight due to intra-band processes, which resides mainly in the far-IR, is strongly suppressed and is transferred to higher frequencies in the mid- and near-IR [3,37-39]. The tendency of the electron localization can be quantified with the spectral weight ratio [39,40]: SW_{intra}/SW_{tot}. The total spectral weight (SW_{tot}) includes the spectral weight of the intra-band absorption (SW_{intra}) as well as the incoherent part in the mid- and near-IR. In our spectra of $Bi_2Ir_2O_7$, SW_{tot} was estimated by integrating the $\sigma_1(\omega)$ up to 1 eV, and SW_{intra} was estimated by subtracting the intensity of the fitted mid-IR resonance from SW_{tot}. We found the SW_{intra}/SW_{tot} value of our material to be about 0.5, which is rather similar to those in many correlated metals [3,41].

The mid-IR absorption in TMOs has been interpreted in various ways: correlation effects, electron-phonon coupling, formation of mid-gap states, charge-density-wave instability, unidirectional charge separation [2,42-44]. The origin of the mid-IR resonance in $Bi_2Ir_2O_7$ is yet to be understood. So far, the electron-phonon coupling has not been given careful consideration in pyrochlore iridates. One possibility is the formation of charge density wave. In this context we note a profound effect of the density wave on the electronic properties of a 5*d* pyrochlore $Cd_2Os_2O_7$ [45] system resulting in the insulating state at *T* below 226 K. We also note that the similar mid-IR absorption was observed in 4*d* Bi-related pyrochlore $(Bi,Y)_2Ru_2O_7$, and was attributed to the mid-gap state formed by the effective doping of the Bi bands near the Fermi level [46]. The mid-gap state has been found in some doped Mott/charge-transfer insulators with large bandgaps, which is not the case of our iridate pyrochlore. Another possible origin of the mid-IR absorption in $Bi_2Ir_2O_7$ is the formation of the Hubbard bands

within the $J_{eff,1/2}$ band due to on-site Coulomb repulsion U [4,5]. While the magnitude of U for 5d Ir-oxides is expected to be below 1 eV [5], the bandwidth of the $J_{eff,1/2}$ band formed by the spin-orbit coupling can also be narrow [4, 5]. Therefore, one can expect that Coulomb effects could play a critical role in determining the electronic structure of Ir-oxides. The observation of the insulator-metal transition in $R_2Ir_2O_7$ compounds suggests the importance of the Coulomb interaction [18-21].

In order to get insights into the nature of the Peak α in $\sigma(\omega)$ of $Bi_2Ir_2O_7$, it is instructive to discuss the evolution of the infrared response of the Ruddlesden-Popper (RP) series $Sr_{n+1}Ir_nO_{3n+1}$, where insulator-to-metal transition occurs with increasing n. In an insulating Sr_2IrO_4, the interband transition within the $J_{eff,1/2}$ bands across the Mott gap is observed at 0.5 eV, in addition to a higher energy of interband transition from the $J_{eff,3/2}$ to the $J_{eff,1/2}$ bands at 1 eV [4,5]. The Hubbard band transition in the $J_{eff,1/2}$ bands shifts to a lower energy down to 0.2 eV for the semi-metallic n=2 phase, and appears to persist in the three-dimensional correlated metal, $SrIrO_3$ with n=∞, even if it is quite weak. Clearly, these 0.2 eV optical transition features in (semi)metallic Ir-oxides in the RP series are quite consistent with Peak α in our conductivity spectra of pyrochlore $Bi_2Ir_2O_7$ [5, 47]. From this common aspect of (semi)metallic iridates, Peak α in $Bi_2Ir_2O_7$ might be assigned as the correlation-induced interband transition. However, at the moment the correlated metallic state in $Bi_2Ir_2O_7$ is not reproduced in the theoretical calculations [22,23]. We note that even the previous LDA+U calculation with $U \leq 2$ eV did not address the correlation-induced band splitting in metallic pyrochlore iridates [23]. Further systematic theoretical studies are required to elucidate the role of the correlation effect in the low-frequency electronic response in $Bi_2Ir_2O_7$.

IV. SUMMARY

We performed infrared measurements on metallic pyrochlore iridate $Bi_2Ir_2O_7$ single crystals, and investigated its electronic structure by analyzing optical conductivity. The two interband transitions from $J_{eff,3/2}$ to $J_{eff,1/2}$ and e_g states are observed at 1.5 and just above 3 eV, respectively. The optical conductivity spectra below 1 eV show a narrow mid-infrared absorption near 0.2 eV. Our studies show that the electronic response of this compound is governed by the strong spin-orbit coupling and the correlation effects. We note that these two ingredients are prerequisite of the non-trivial topological ground state in pyrochlore iridates. We also suggest the possible existence of the lowest frequency suppression in the optical conductivity of our compound, which might be a common feature of metallic pyrochlore iridates.

ACKNOWLEDGEMENTS

Work performed at UCSD was supported by the DOE-BES. YSL was supported by the Soongsil University Research fund, and by the National Research Foundation of Korea (NRF) grant funded by the Korea government (MEST) (No. 2012-0005052). Work performed at Stanford University was supported by the DOE under Contract No. DE-AC02-76SF00515. JYC acknowledges NSF-DMR 1063735 for partial support. AFK was supported by the U.S. Department of Energy, Basic Energy Sciences, Materials Sciences and Engineering Division under contract No. DE-AC02-76SF00515. SJM was supported by from Basic Science Research Program through the National Research Foundation of Korea funded by the Ministry of Education, Science, and Technology (2012R1A1A1013274).

APPENDIX: X-ray diffraction analysis on $Bi_2Ir_2O_7$

Crystallographic data were collected initially at room temperature on a Nonius KappaCCD single crystal diffractometer using Mo Kα radiation (λ = 0.72073 Å). The crystal structure of $Bi_2Ir_2O_7$ was solved by direct methods using SIR97 [48] and refined using SHELXL97 [49]. The final model

contains anisotropically modeled atomic displacement parameters and extinction corrections. Crystallographic parameters, atomic positions, anisotropic thermal parameters, and interatomic distances are given in TABLE I.

Diffraction images collected on the Nonius diffractometer showed very low intensity peaks resulting from high absorption of Mo Kα radiation by the sample. Consequential refinement of crystallographic models contained unreasonably large and directionally anisotropic thermal parameter values for the oxygen atoms. Increasing sample size and X-ray beam exposure time proved to be an inefficient means of solving this problem, and so single crystal diffraction data were also collected at the Advanced Light Source at the Lawrence Berkeley National Laboratory for further structural elucidation.

Crystallographic data were also collected at 150 K on a D8 goniostat equipped with APEXII CCD detector at Beamline 11.3.1 at the Advanced Light Source at the Lawrence Berkeley National Laboratory using synchrotron radiation tuned to λ = 0.7749 Å. Frames were measured for 3 s at 0.5° intervals of ω with a maximum 2θ of ~60°. Data were collected using the APEX2 program and processed using the SAINT program routine within the APEX2 software. The data were corrected for adsorption and beam corrections based on the multi-scan technique as implemented by SADABS. Structural models were refined using the SHELXL97 [49] program. Structural models were corrected for extinction and refined with anisotropic atomic displacement parameters. Crystallographic parameters, atomic positions and displacement parameters, anisotropic thermal parameters, and interatomic distances are given in TABLE I.

$Bi_{1.94(1)}Ir_2O_{6.91(3)}$ adopts the pyrochlore structure type ($Fd\bar{3}m$ space group) and has the lattice parameter a = 10.312(7) Å. Upon refinement of the model solved from data collected at the Advanced Light Source, it was found that occupancies on the Bi and O2 sites return slight deviations from full occupancy, giving the compound the chemical formula $Bi_{1.94(1)}Ir_2O_{6.91(3)}$. The occupancy is similar to the previously reported structure solved from neutron diffraction data [50]. The increased radiation

intensity at the Advanced Light Source proved crucial in determining the oxygen vacancies present in this compound, as no partial occupancy on any site was discernible for all crystallographic models solved using data collected on the laboratory instrument. Values for Bi-O and Ir-O bond distances are in agreement with previously reported distances [50] and indicate that Ir is in the +4 oxidation state and that Bi is in the +3 oxidation state.

REREFENCES

[1] P. A. Cox, Transition metal oxides (Clarendon, Oxford, 1992).

[2] M. Imada, A. Fujimori, and Y. Tokura, Rev. Mod. Phys. **70**, 1039 (1998).

[3] D. N. Basov, R. D. Averitt, D. van der Marel, M. Dressel, K. Haule, Rev. Mod. Phys. **85**, 471 (2011).

[4] B. J. Kim, Hosub Jin, S. J. Moon, J.-Y. Kim, B.-G. Park, C. S. Leem, Jaejun Yu, T. W. Noh, C. Kim, S.-J. Oh, V. Durairai, G. Cao, and J.-H. Park, Phys. Rev. Lett. **101**, 076402 (2008).

[5] S. J. Moon, H. Jin, K. W. Kim, W. S. Choi, Y. S. Lee, J. Yu, G. Cao, A. Sumi, H. Funakubo, C. Bernhard, and T. W. Noh, Phys. Rev. Lett. **101**, 226401 (2008).

[6] O. B. Korneta, Tongfei Qi, S. Chikara, S. Parkin, L. E. De Long, P. Schlottmann, and G. Cao, Phys. Rev. B **82**, 115117 (2010).

[7] T. F. Qi, O. B. Korneta, L. Li, K. Butrouna, V. S. Cao, Xiangang Wan, P. Schlottmann, R. K. Kaul, and G. Cao, Phys. Rev. B **86**, 125105 (2012).

[8] G. Cao, J. E. Crow, R. P. Guertin, P. F. Henning, C. C. Homes, M. Strongin, D. N. Basov, and E. Lochner, Solid State Commun. **113**, 657 (2000).

[9] S. Nakatsuji, Y. Machida, Y. Maeno, T. Tayama, T. Sakakibara, J. van Duijn, L. Balicas, J. N. Millican, R. T. Macaluso, and Julia Y. Chan, Phys. Rev. Lett. **96**, 087204 (2006).

[10] Y. Machida, S. Nakatsuji, S. Onoda, T. Tayama, and T. Sakakibara, Nature **463**, 210 (2010).

[11] Atsuo Shitade, Hosho Katsura, Jan Kuneš, Xiao-Liang Qi, Shou-Cheng Zhang, and Naoto Nagaosa, Phys. Rev. Lett. **102**, 256403 (2009).

[12] Jean-Michel Carter, V. Vijay Shankar, M. Ahsan Zeb, and Hae-Young Kee, Phys. Rev. B **85**, 115105 (2012).

[13] D. A. Pesin and Leon Balents, Nature Phys. **6**, 376 (2010).

[14] Bohm-Jung Yang and Yong Baek Kim, Phys. Rev. B **82**, 085111 (2010).

[15] Xiangang Wan, Ari M. Turner, Ashvin Vishwanath, and Sergey Y. Savrasov, Phys. Rev. B **83**, 205101 (2011).

[16] Ara Go, William Witczak-Krempa, Gun Sang Jeon, Kwon Park, and Yong Baek Kim, Phys. Rev. Lett. **109**, 066401 (2012).

[17] F. F. Tafti, J. J. Ishikawa, A. McCollam, S. Nakatsuji, and S. R. Julian, Phys. Rev. B **85**, 205104 (2012).

[18] D. Yanagishima and Y. Maeno, J. Phys. Soc. Jpn. **70**, 2880 (2001).

[19] K. Matsuhira, M. Wakeshima, R. Kakanishi, and T. Yamada, J. Phys. Soc. Jpn. **76**, 043706 (2007).

[20] Jun J. Ishikawa, Eoin C. T. O'Farrel,and Satoru Nakatsuji, arXiv:1203.4182.

[21] K. Ueda, J. Fujioka, Y. Takahashi, T. Suzuki, S. Ishiwata, Y. Taguchi, and Y. Tokura, Phys. Rev. Lett. **109**, 136402 (2012).

[22] Yasuyuki Hirata, Makoto Nakajima, Yusuke Nomura, Hiroyuki Tajima, Yoshitaka Matsushita, Keiko Asoh, Yoko Kiuchi, Adolfo G. Eguiluz, Ryotaro Arita, Tohru Suemoto, and Kenya Ohgushi, arXiv:1201.6410.

[23] T. F. Qi, O. B. Korneta, Xiangang Wan, L. E. DeLong, P. Schlottmann, and G. Cao, J. Phys.: Condens. Matter **24**, 345601 (2012).

[24] Scott. C. Riggs *et al*., in preparation.

[25] R. D. Shannon, Acta Cryst. **A32**, 751 (1976).

[26] Beverly Brooks Hinojosa, Juan C. Nino, and Aravind Asthagiri, Phys. Rev. B **77**, 104123 (2008).

[27] J. Chu, private communications.

[28] Makoto Tachibana, Yoshimitsu Kohama, Tomotaka Shimoyama, Akihiro Harada, Tomoyasu Taniyama, Mitsuru Itoh, Hitoshi Kawaji, and Tooru Atak, Phys. Rev. B **73**, 193107 (2006).

[29] C. C. Homes, M. Reedyk, D. A. Crandles, and T. Timusk, Appl. Opt. **32**, 2976 (1993).

[30] F. Wooten, Optical Properties of Solids (Academic, New York, 1972).

[31] D.N. Basov, A.V. Puchkov, R.A. Hughes, T. Strach, J. Preston, T. Timusk, D.A. Bonn, R. Liang, and W.N. Hardy, Phys. Rev. B **49**, 12165 (1994).

[32] D.N. Basov, B. Dabrowski, and T. Timusk, Phys. Rev. Lett. **81**, 2132 (1998).

[33] M. Dumm, S. Komiya, Y. Ando, and D. N. Basov, Phys. Rev. Lett. **91**, 077004 (2003).

[34] S. Lupi, D. Nicoletti, O. Limaj, L. Baldassarre, M. Ortolani, S. Ono, Yoichi Ando, and P. Calvani, Phys. Rev. Lett. **102**, 206409 (2009).

[35] Andrew L. Hector and Seth B. Wiggin, J. Solid State Chem. **177**, 139 (2004).

[36] Stuart J. Henderson, Olga Shebanova, Andrew L. Hector, Paul F. McMillan, and Mark T. Weller, Chem. Mater. **19**, 1712 (2007).

[37] M. M. Qazilbash, J. J. Hamlin1, R. E. Baumbach, Lijun Zhang, D. J. Singh, M. B. Maple, and D. N. Basov, Nature Physics **5**, 647 (2009).

[38] S. J. Moon, A. A. Schafgans, S. Kasahara, T. Shibauchi, T. Terashima, Y. Matsuda, M. A. Tanatar, R. Prozorov, A. Thaler, P. C. Canfield, A. S. Sefat, D. Mandrus, and D. N. Basov. Phys. Rev. Lett. **109**, 027006 (2012).

[39] L Degiorgi, New J. Phys. **13**, 023011 (2011).

[40] J. L. M. van Mechelen, D. van der Marel, C. Grimaldi, A. B. Kuzmenko, N. P. Armitage, N. Reyren, H. Hagemann, and I. I. Mazin, Phys. Rev. Lett. **100**, 226403 (2008).

[41] D. N. Basov and Andrey V. Chubukov, Nature Phys. **7**, 272 (2011).

[42] G. Gruner, Density waves in Solids (Addison-Wesley, Reading, MA, 1994).

[43] D. N. Basov and T. Timusk, Rev. Mod. Phys. **77**, 721 (2005).

[44] Y. S. Lee, Kouji Segawa, Z. Q. Li, W. J. Padilla, M. Dumm, S. V. Dordevic, C. C. Homes, Yoichi Ando, and D. N. Basov, Phys. Rev. B **72**, 054529 (2005).

[45] W. J. Padilla, D. Mandrus, and D. N. Basov, Phys. Rev. B **66**, 035120 (2002).

[46] J. S. Lee, S. J. Moon, T. W. Noh, T. Takeda, R. Kanno, S. Yoshii, and M. Sato, Phys. Rev. B **72**, 035214 (2005).

[47] S. Y. Jang, H. Kim, S. J. Moon, W. S. Choi, B. C. Jeon, J. Yu, and T. W. Noh, J. Phys. Condens. Matter **22**, 485602 (2010).

[48] A. Altomare, M. C. Burla, M. Camalli, G. L., Cascarano, C. Giacovazzo, A. Guagliardi, A. G. G. Moliterni, G. Polidori, R. J. Spagna, J. Appl. Crystallogr. **32**, 115 (1999).

[49] G. Sheldrick, Acta Cryst. A **64**, 112 (2008).

[50] B. J. Kennedy, J. Solid State Chem. **123**, 14 (1996).

TABLE

TABLE I. Crystallographic parameters for $Bi_2Ir_2O_7$ compounds.

Crystal data		
Formula	**$Bi_2Ir_2O_7$**	**$Bi_{1.94(1)}Ir_2O_{6.91(3)}$ (synch)**
Space group	*Fd* -3*m*	*Fd* -3*m*
a (Å)	10.314(3)	10.312(7)
V (Å^3)	1197.3(5)	1196.6(12)
Z	8	8
Crystal size (mm)	0.10 x 0.10 x 0.10	0.002 x 0.005 x 0.10
Temperature (K)	294(2)	150(2)
Density (g cm^{-3})	11.070	10.910
θ Range (°)	5.59-33.67	3.73-30.92
μ (mm^{-1})	112.297	125.486
Data Collection and Refinement		
Collected reflections	6470	2306
Unique reflections	170	85
R_{int}	0.072	0.1102
h	$2 \le h \le 15$	$-13 \le h \le 13$
k	$0 \le k \le 10$	$-13 \le k \le 13$
l	$0 \le l \le 10$	$-13 \le l \le 13$
$\Delta\rho_{max}$ (e Å^{-3})	1.658	2.180
$\Delta\rho_{min}$ (e Å^{-3})	-1.563	-4.001
GoF	1.287	1.199
Extinction coefficient	0. 23(10)	0. 00033(8)
[a] $R_1(F)$ for $F_o^2 > 2\sigma(F_o^2)$	0.0256	0.0391
[b] $R_w(F_o^2)$	0.0845	0.0814

[a] $R_1 = \Sigma||F_o| - |F_c||/\Sigma|F_o|$

[b] $wR_2 = [\Sigma w(F_o^2 - F_c^2)^2/\Sigma w(F_o^2)^2]^{1/2}$; $w = 1/[\sigma^2(F_o^2) + 0.0443P^2 + 35.4143P]$ at 294 K for $Bi_2Ir_2O_7$ and $w = 1/[\sigma^2(F_o^2) + 0.0353P^2 + 2.7862P]$ at 150 K for $Bi_{1.94(1)}Ir_2O_{6.91(3)}$.

Figure Captions.

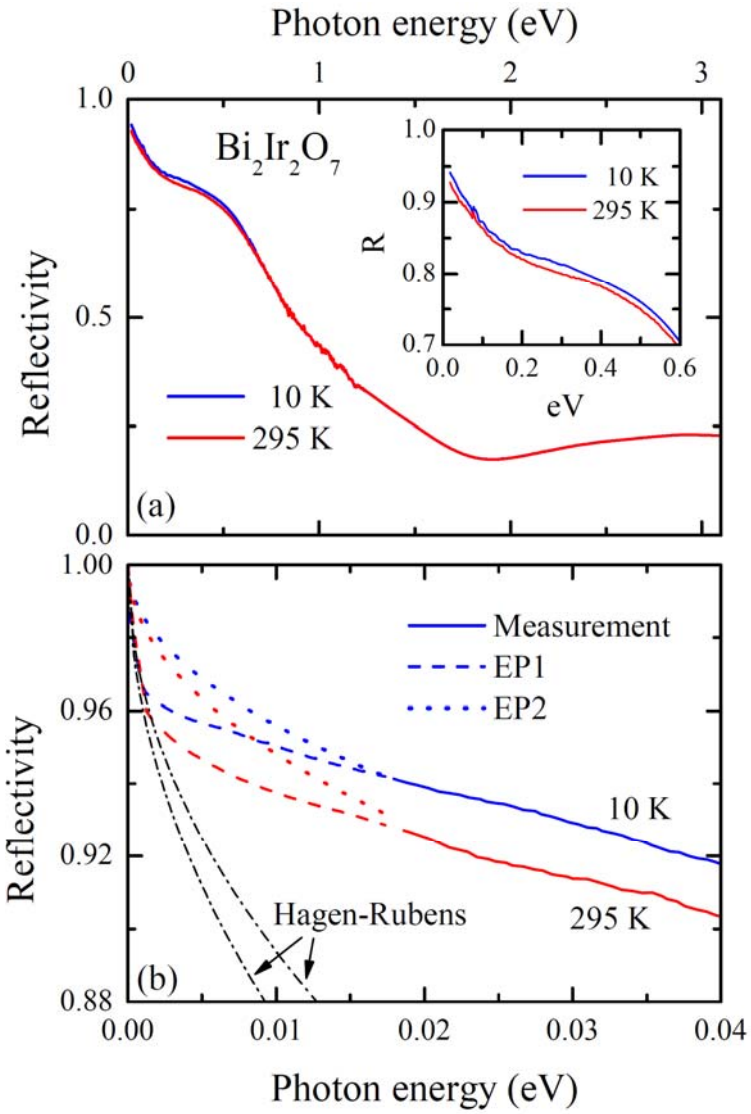

Fig. 1. (Color online) (a) Temperature dependent reflectivity spectra $R(\omega)$ of $Bi_2Ir_2O_7$. (b) Far-IR $R(\omega)$ below 0.04 eV. The solid lines represent the experimental data. Two extrapolation lines, denoted as EP1 and EP2, are represented by the dotted and dashed lines, respectively. The dot-dashed lines are the H-R lines with ρ_{DC} =104 and 145 mΩcm for the 10 K and 295 K data, respectively.

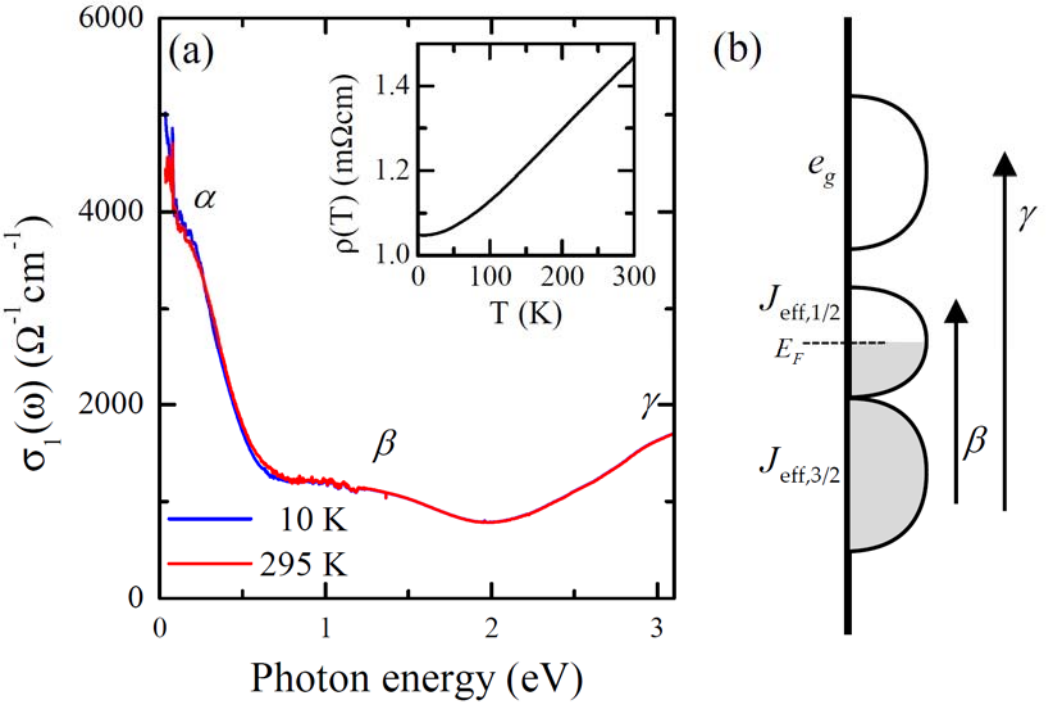

Fig. 2 (a) (Color online) Temperature dependent optical conductivity spectra $\sigma_1(\omega)$ of $Bi_2Ir_2O_7$. Three interband transitions are denoted with Peak α, Peak β, and Peak γ from the lowest peak energy. Inset: DC resistivity curve of $Bi_2Ir_2O_7$. (b) Schematic diagram of the band structure for $Bi_2Ir_2O_7$. Peak β and Peak γ denote the transition from $J_{eff,3/2}$ to $J_{eff,1/2}$ and e_g bands, respectively.

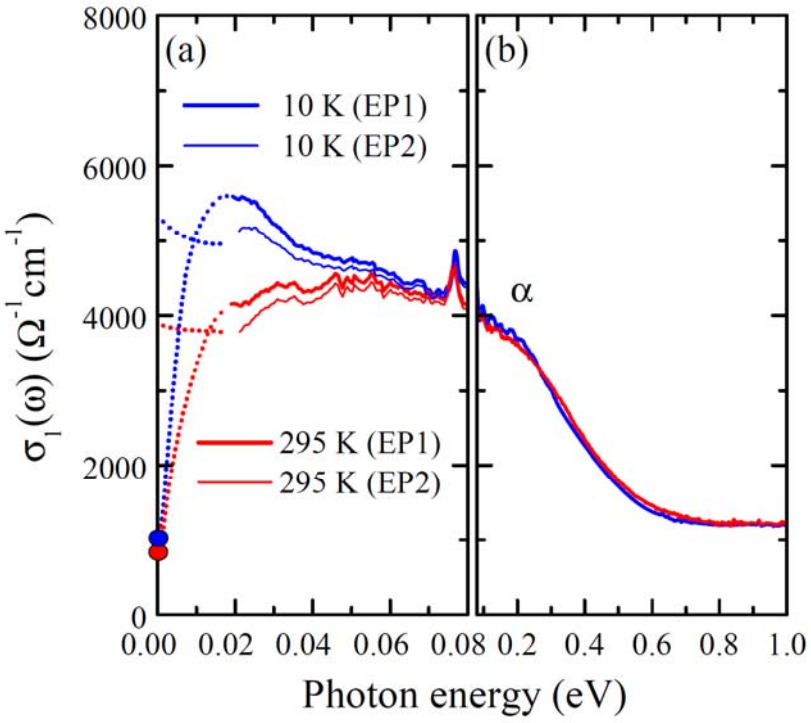

Fig. 3 (a) (Color online) Far-IR $\sigma(\omega)$ below 0.08 eV. The thick and thin solid lines represent the optical conductivity data calculated using EP1 and EP2 extrapolations, respectively. The dotted lines represent the optical conductivity data in the extrapolation region. The circle symbols on the *y* axis indicate the DC conductivity values estimated from the transport measurement. The sharp features near 0.08 eV are optical phonons which show quite weak temperature dependence. (b) Optical conductivity data in photon energy of 0.08 – 1 eV for clear view of Peak α.